Spectroscopic diagnostics for liquid lithium divertor studies on National Spherical Torus Experiment[a)]

V. A. Soukhanovskii,[1,b)] A. L. Roquemore,[2] R. E. Bell,[2] R. Kaita,[2] and H. W. Kugel[2]
[1]*Lawrence Livermore National Laboratory, Livermore, California 94551, USA*
[2]*Princeton Plasma Physics Laboratory, Princeton, New Jersey 08543, USA*

(Presented 18 May 2010; received 17 May 2010; accepted 26 June 2010; published online 20 October 2010)

The use of lithium-coated plasma facing components for plasma density control is studied in the National Spherical Torus Experiment (NSTX). A recently installed liquid lithium divertor (LLD) module has a porous molybdenum surface, separated by a stainless steel liner from a heated copper substrate. Lithium is deposited on the LLD from two evaporators. Two new spectroscopic diagnostics are installed to study the plasma surface interactions on the LLD: (1) A 20-element absolute extreme ultraviolet (AXUV) diode array with a 6 nm bandpass filter centered at 121.6 nm (the Lyman-α transition) for spatially resolved divertor recycling rate measurements in the highly reflective LLD environment, and (2) an ultraviolet-visible-near infrared $R=0.67$ m imaging Czerny–Turner spectrometer for spatially resolved divertor D I, Li I-II, C I-IV, Mo I, D_2, LiD, CD emission and ion temperature on and around the LLD module. The use of photometrically calibrated measurements together with atomic physics factors enables studies of recycling and impurity particle fluxes as functions of LLD temperature, ion flux, and divertor geometry. © *2010 American Institute of Physics.* [doi:10.1063/1.3478749]

I. INTRODUCTION

The use of lithium coatings evaporated on graphite plasma facing components (PFCs) has been under investigation for plasma density control and performance improvements in the National Spherical Torus Experiment (NSTX).[1,2] Recently, a liquid lithium toroidal module was installed in the NSTX lower divertor area. The liquid lithium divertor (LLD) module has a porous molybdenum surface, separated by a stainless steel liner from a copper substrate.[3] Lithium is deposited on the LLD surface from two overhead evaporators.[1] A perceived advantage of the LLD over the solid lithium coating is a self-regenerating lithium surface for pumping hydrogenic fuel ions and atoms.

In order to assess the relationship between lithium-coated and liquid lithium divertor surface conditions and edge-core plasma transport and radiation properties, the NSTX diagnostics complex has been augmented with a new array of divertor Langmuir probes at the LLD radial location,[4] a material analysis and particle probe, a two color infrared thermography system, and a charge-exchange recombination spectroscopy system[5] upgraded for core lithium density measurements. In this paper, we describe two new divertor diagnostics that are being installed on NSTX: (1) A Lyman-α (Ly_α) diode array (here forth referred to as LADA), and (2) an ultraviolet-visible-near infrared (UV-VIS-NIR) divertor imaging spectrometer (here forth referred to as DIMS). These diagnostics will contribute to the planned studies of retention and recycling of deuterium as a function of LLD surface conditions (e.g., Li coverage and temperature), divertor T_e and n_e, strike point proximity, and flux expansion, as well as to relate the LLD surface temperature to the measured influx of impurity and hydrogenic species.

II. METHOD

Plasma operations with evaporated lithium coatings in NSTX bring up a number of diagnostic concerns. The concerns include (1) degradation in transmission of diagnostic port windows and reflectivity of in-vessel mirrors due to exposure to lithium fluxes, (2) deposition of lithium on exposed diagnostic parts (e.g., foil filters and probe surfaces), and (3) large changes in the dynamic range of some measured quantities (e.g., edge neutral pressure, n_e and recycling) due to lithium pumping. These concerns are generally addressed by diagnostic hardware modifications or additional calibration efforts.

Evaporated lithium coatings can also affect measurements directly, for example, reflections of light from the LLD surface can complicate the interpretation of the VIS and IR spectroscopy. To understand the impact of reflections, the reflectivities of common fusion PFCs (e.g., graphite and molybdenum) are characterized in the laboratory and incorporated in numerical diagnostic models.[6,7] Reflectivities of lithium-coated PFCs, however, have not been studied. While laboratory data in this case may help interpret visible spectroscopic measurements from the LLD, the impact of a dynamic, real-time variation in the LLD surface conditions would still be a concern. In NSTX, lithium coatings evaporated on graphite PFCs tended to increase surface reflectivity, as was apparent in the VIS and IR camera measurements.

[a)]Contributed paper, published as part of the Proceedings of the 18th Topical Conference on High-Temperature Plasma Diagnostics, Wildwood, New Jersey, May 2010.
[b)]Electronic mail: vlad@llnl.gov.

TABLE I. Candidate spectral lines for divertor deuterium and impurity flux measurements in NSTX.

Species	Wavelength (nm)
D Balmer series	376.9, 379.7, 383.4, 388.8, 396.9, 410.0, 433.9, 486.0, 656.1
D_2 Fulcher band $d\ ^3\Pi_u - a\ ^3\Pi_g^+$	592–602
He I	388.9, 587.5, 667.8, 706.7, 1083.0
He II	320.3, 468.5, 541.1
Li I	323.3, 413.2, 460.3, 610.4, 670.8
Li II	319.9, 325.0, 467.8, 478.9, 548.5
LiD band $A\ ^1\Sigma^+ - X\ ^1\Sigma^+$	330–470
Li_2 band $B\ ^1\Pi_u - X\ ^1\Sigma_g^+$	460–550
C I	493.2, 538.0, 833.5, 909.4,1175.4
C II	392.0, 426.7, 514.0, 658.0, 678.0, 723.0
C III	407.0, 465.0, 569.6, 833.2, 850.0
C IV	465.8, 580.1
CD band $A^2\Delta - X^2\Pi$	431
CD band $B^2\Sigma - X^2\Pi$	390
Fe I	344.1, 358.1, 372.0, 649.5
Mo I	379.8, 386.4, 390.2, 550.6, 553.3, 557.0

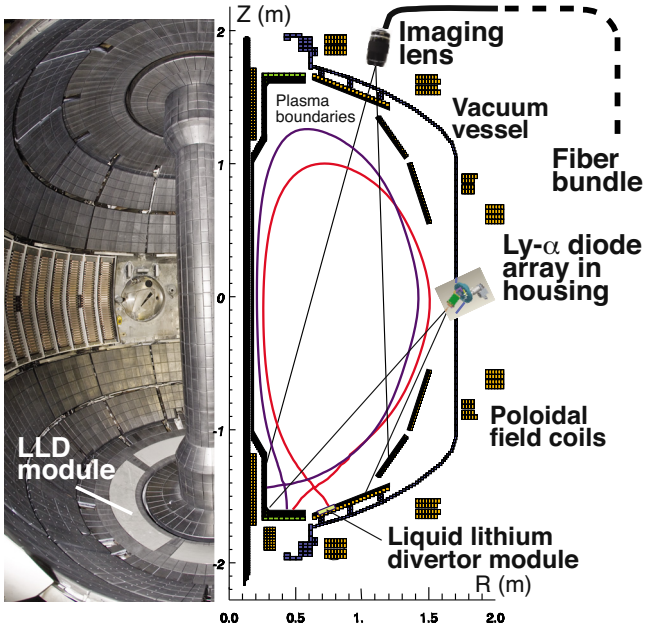

FIG. 1. (Color online) Placement of the LADA and DIMS diagnostics on NSTX. Their divertor views are shown by thin lines.

The LLD module was designed to operate at temperatures up to 350 °C, well above the lithium melting point 180 °C. Liquid lithium surface has a mirrorlike appearance with high reflectivity in the VIS range.[8] According to Ref. 9 data, the reflectance of liquid lithium at normal incidence is 0.5–0.95 throughout the visible range, 0.3–0.5 in the UV range, and ≤ 0.01 in the far-UV range. This motivated us to consider spectroscopic measurements in the near and far-UV range, where reflectivities are low.

Photometrically calibrated spectroscopy and the S/XB technique[10] will be used for plasma-LLD interaction analysis, measurements of recycling, and impurity particle fluxes. The S/XB technique relates spectral line intensities to particle influx using the ionizations per photon factors S/XB [where S and X are the ionization and excitation rates and B is the branching ratio (a ratio of radiative transition probabilities) for the spectral line used] from collisional-radiative model calculations or laboratory measurements. The S/XB technique assumes that the ionization and excitation processes occur in a common plasma volume characterized by T_e and n_e. Independent local T_e and n_e measurements with, e.g., Langmuir probes, are therefore of high priority since the S/XB factors are generally T_e and n_e-dependent. Using the divertor ionization flux Γ_i^{out} inferred from the visible Balmer-α, β, far-UV Ly_α emission line intensities, and the ion flux incident on the divertor surface Γ_i^{in} from the Langmuir probes,[4] a local recycling coefficient $R=\Gamma_i^{\text{out}}/\Gamma_i^{\text{in}}$ can be estimated. This is particularly important for numerical modeling of the LLD experiments. The recycling coefficient R is presently used in two-dimensional (2D) edge transport fluid codes as a free input parameter to model the impact of lithium on scrape-off layer plasma transport.[11] To assess PFC impurity fluxes, the emission lines listed in Table I will be used. For deuterium and main NSTX plasma impurities abundant S/XB data are available in the ADAS database[12] and literature.

III. LYMAN α DIODE ARRAY

The objective of the LADA diagnostic is to measure neutral deuterium emission from the divertor region while minimizing parasitic contributions from reflections off the LLD module. For this reason, the deuterium Ly_α $n=2-1$ resonant line at $\lambda=121.6$ nm (in the far-UV) was selected. The measurements will be compared to those from the existing photometrically calibrated $D_{\alpha,\beta,\gamma}$ cameras.[13] The LADA diagnostic by its design is a filtered pinhole camera with a one-dimensional array detector: an absolute extreme ultraviolet silicon diode array from International Radiation Detectors, Inc. With proper handling and accurate accounting of the diagnostic factors (such as etendue, transmission, diode response, and electronic gain factors), AXUV diode measurements are interpreted in absolute photometric units. A number of diagnostics based on AXUV diodes, including those for Ly_α measurements, have been implemented on magnetically-confined fusion (MCF) plasma devices.[14–21]

The LADA diagnostic is mounted on a 6 in. vacuum flange placed in the equatorial plane of the NSTX vacuum vessel (Fig. 1). The diagnostic layout is shown in Fig. 2. The in-vacuum diagnostic housing encloses a stainless steel block with a copper insert holding a precision slit disk and a spectral bandpass filter, and the diode array. The twenty element model AXUV20EL array is a compromise between the diode sensitive area (3 mm^2) and the diode element capacitance (nominally 1 nF) for an acceptable signal-to-noise ratio. The AXUV diode sensitivity is 0.11 A/W at $\lambda=121.6$ nm. The slit area is 2 mm^2 and it is placed 10 cm from the diode array. Each diode element forms a monochromator with an etendue $\simeq 6\times 10^{-10}$. For Ly_α spectral filtering, the open-faced Acton Research Corp. filter Type 122-XN-.5D mounted on a 12.5 mm diameter MgF_2 substrate is used. The filter has a peak transmission 0.055 and the measured bandpass [full width at half maximum (FWHM)] 9.2 nm centered

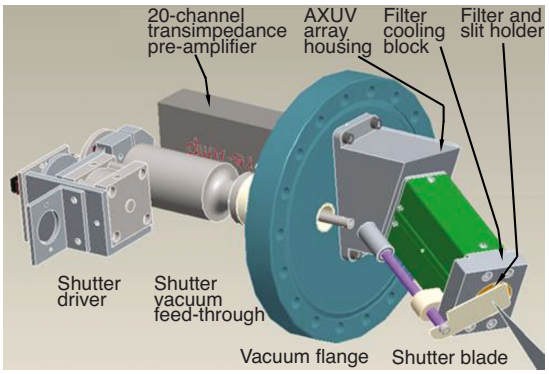

FIG. 2. (Color online) Lyman-α diode array schematic.

on the Ly_α line. No strong impurity lines are within the bandpass,[15] except the Li III $n=6-3$ line at $\lambda=121.6$ nm which is not expected to be strong in the divertor region. In order to keep the filter temperature at $T\leq 50-60$ °C during the NSTX vacuum vessel bake-out and LLD high-temperature operation, the stainless steel block with the copper insert and the filter are water-cooled. The cooling tubes are welded to the 6 in. mounting flange and form a loop inside the block. A remotely controlled shutter is used to protect the slit and the filter from the line-of-sight lithium atoms evaporated from the LLD. The AXUV20EL array is connected to a preamplifier through a multipin DB-shell vacuum feed through. The twenty channel dc-coupled transimpedance preamplifier Model 8986A built by Clear-Pulse, Inc. is mounted on the air side of the diagnostic. The preamplifier characteristics are: gain 10^6, frequency response 10 kHz, and output impedance 50Ω. A twisted-pair shielded cable is used to transmit analog signals to a 96-channel digitizer module model ACQ196CPCI from D-TACQ Solutions Ltd. The digitizer module provides 16-bit digitization at 500 kSPS/channel and sends digital data directly to a MDS Plus server, eliminating a need for an additional personal computer (PC).

The LADA diagnostic has been installed in NSTX and electronic background noise data in the range $\pm(10-40)$ mV has been recorded in initial NSTX 2010 campaign discharges. The thermal (Johnson) noise was estimated to be in the microvolt range. The expected Ly_α signals were estimated from the measured divertor D_α intensity and ADAS photon emission coefficients to be in the range 0.5–5 V.

IV. DIVERTOR IMAGING SPECTROMETER

The objective of the DIMS diagnostic is to provide centimeter-scale spatially resolved divertor profile measurements of (1) deuterium and impurity atomic and molecular emissions and (2) divertor ion temperature T_i based on Doppler spectral line broadening. The term "imaging spectrometer" is used here to describe the concept of collecting light from several localized spatial regions in the divertor, relaying the light via separate fibers to the spectrometer entrance slit, and focusing the dispersed light on a 2D detector, while minimizing aberrations. Measurements by an existing

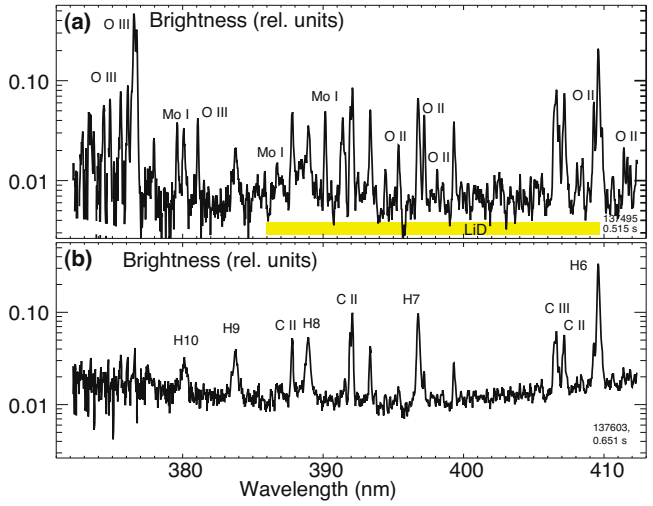

FIG. 3. (Color online) UV spectra recorded from a LLD view by an existing divertor spectrometer in initial LLD experiments: (a) when a large MHD mode plasma hit the lower divertor and (b) with LLD at 320 °C.

ten-chord divertor imaging spectrometer[22] provided many important contributions to NSTX divertor studies,[22–25] as well as insights for the design of the new system.

Particularly important for LLD protection will be the operational monitoring of metal influx from the LLD. This will be accomplished by high spectral resolution measurements in the UV spectral region (≤400 nm). The presence of molybdenum (Mo I-II) or iron (Fe I-III) lines (e.g., Table I) in the divertor spectra may be indicative of a direct plasma interaction with the LLD substrate and steel liner caused by insufficient lithium coating of the LLD surface. To illustrate this, Fig. 3 shows the UV spectra measured by the existing divertor spectrometer[22] with spectral resolution $\lambda/\delta\lambda\leq 4000$ in the initial LLD experiments. Molybdenum and iron lines were not measured routinely in discharges with the outer divertor strike point close to the LLD. In several discharges, the three Mo I lines (at 379.8, 386.4, and 390.2 nm) were identified in the fiber channel viewing the LLD module, following a large magnetohydrodynamic event that impacted the cold ($T=20-30$ °C) LLD. Also observed in the 380–410 nm range were molecular lines from the LiD band $A\ ^1\Sigma_+-X\ ^1\Sigma_+$. In earlier NSTX experiments the CD B-X band and BD bands were observed in the same spectral range.[22] Generally, these molecular band lines complicated atomic spectra interpretation. However, the molecular spectra can also contribute to understanding of LLD surface processes that depend on LLD temperature and surface conditions. A number of lithium deuteride, lithium carbonate, and lithium oxide compounds can form on the LLD surface affecting the reactions between ionized and neutral deuterium with lithium. For example, in 3 MW neutral beam injection (NBI)-heated discharges with the LLD operated at $T\simeq 320$ °C, a decrease in intensities of molecular and low Z impurity (C and O) lines was apparent, suggesting the clean-up of the LLD module surface [Fig. 3(b)].

Nearly stigmatic, aberration-free, high spectral resolution imaging imposes challenging requirements on the diagnostic parameters and elements. The DIMS diagnostic has been designed as a system built from commercial compo-

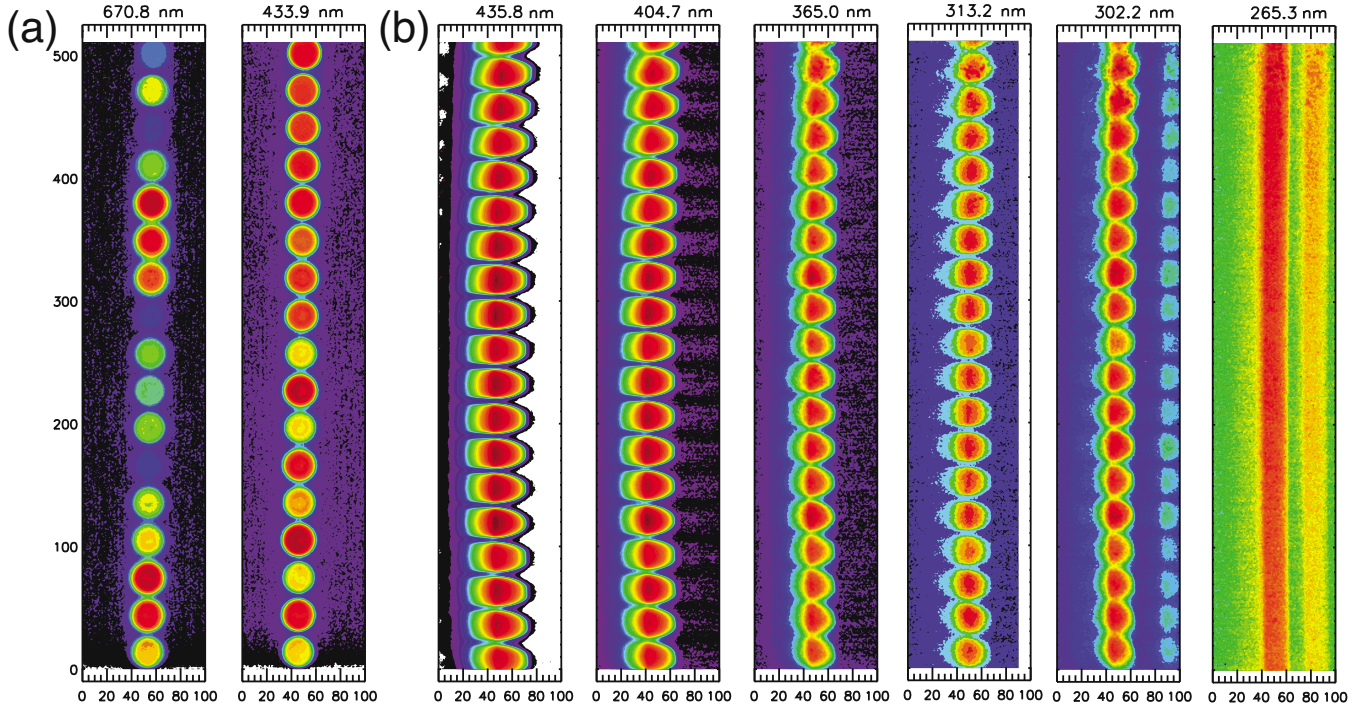

FIG. 4. (Color online) (a) False-color images of input optics fibers focused with the DIMS achromatic triplets at λ670.8 nm and λ433.9 nm. Irregularities in fiber illumination were due to uneven source distribution. (b) Series of imaging UV spectra of Hg lines (wavelengths shown on top of each panel).

nents that maximizes throughput yet minimizes astigmatism and chromatic aberrations in a broad UV-VIS-NIR spectral range. The system consists of an imaging lens, a fiber optic relay bundle, a spectrometer input fiber bundle, input imaging optics, and a spectrometer with a charge-coupled device (CCD) detector. Each of these components was selected to provide good transmission, sensitivity, or achromatic imaging in a broad spectral range 200–1100 nm. In addition, the overall system etendue (system $F/\#=4.7$) was optimized by matching $F/\#$s of all individual components. Below we describe the DIMS in detail.

A. Divertor imaging and relay optics

A six-element lens (model UV-105–4.5 Rayfact from Tochigi Nikon Inc.) with $f=105$ mm, $F/\#=4.5$ provides chromatically corrected imaging and 0.70–0.80 transmission in the range 220–900 nm. The lens is mounted on a sapphire window port at a distance 3.4 m from the divertor surface (Fig. 1). The depth of field in the object plane is 10–20 cm, thereby accommodating the variation in divertor shape. The acceptance angle $\gamma=23.3°$ enables a full view of the divertor with magnification $M\simeq 28$ and millimeter scale spatial resolution. A fiber array holder is mounted in the focal plane of the lens. The holder accommodates two parallel arrays of fibers: a new array of 48 silica-silica 400 μm diameter fibers from Polymicro, Inc. and an old array[22] of 24 quartz 600 μm diameter fibers from Fiberguide. Each 400 μm fiber collects light from a 1 cm spot on the divertor. The UV-VIS-NIR transmission characteristics of the Polymicro type FBP400440480 fibers in the 275–2100 nm range are superior to most available silica-silica high OH content fibers. The numerical aperture of each fiber is 0.22 ($F/\#=2.27$). Both 30 m long fiber bundles relay light from the NSTX Test Cell to a remote radiation-shielded diagnostic room, where each fiber is terminated with an SMA-type connector.

B. Input optics and spectrometer

In the diagnostic room, some of the relay fibers are coupled to the spectrometer input fiber optic bundle via SMA connectors mounted in a switch-board box. The 4 m long input fiber bundle consists of 20 fibers of the same Polymicro type. The bundle is terminated with a custom-made ferrule where the polished fiber ends form a linear array. The array is imaged 1:1 by the input optics on the entrance slit of the spectrometer. Two 30 mm diameter $F/\#=2.0$ infinite-conjugate achromatic triplet lenses from Edmund Optics are used in the input optics assembly. The lenses are designed for a consistent (nearly constant) focal length in the spectral range 200–1000 nm. The spectrometer system consists of the McPherson Inc. Model 207 $R=0.67$ m Czerny–Turner monochromator and a CCD detector. The monochromator is equipped with large 120×140 mm^2 gratings yielding the highest commercial $F/\#=4.7$ for the focal length class. The Model 207 monochromator is also equipped with a master cylinder correcting mirror placed at the exit port to help correct imaging aberrations from spherical mirrors. Since the region of high-quality stigmatic imaging in the detector plane (in the dispersion direction) is limited, the extent of spectral domain on the CCD was not a priority. To provide high-quality imaging and high CCD read out speed, we selected the Princeton Instruments camera Model Pro EM 512. The CCD camera has a square 512×512 chip with 16×16 μm^2 pixels. The back-illuminated e2v CCD97 chip based CCD camera incorporates the latest CCD technology features: an electron multiplication technology resulting in

high quantum efficiency and a frame-transfer architecture with an up to 10 MHz read out rate and 16-bit digitization. The CCD quantum efficiency in the UV range is enhanced by the Unichrome coating. A rack-mounted PC is used to control the monochromator wavelength drive via an RS-232 interface, and to read out the CCD camera data via a gigabit-ethernet cable using the WINSPEC software.

For high-resolution Doppler spectroscopy, three gratings with 3600, 2400, and 1800 gr/mm will be used. Nominal spectral resolution of the Model 207 monochromator with the 3600 (1800) gr/mm grating is 0.012 (0.020) nm and the dispersion is 0.43 (0.83) nm/mm. Typically, 4 pixels per line is sufficient for a reliable Gaussian fit to the data, yielding 0.064 mm FWHM on the CCD as a minimum requirement for the instrumental function width. For the 3600 gr/mm grating, the instrumental FWHM is 0.028 nm, enabling sufficient resolution to measure, e.g., T_i=3–5 eV of D and He atoms (ions) and T_i=5–10 eV of Li and C atoms (ions). However, when a monochromator is used for imaging with a cylinder mirror, its resolution is slightly degraded. Spectral resolution tests of the DIMS diagnostic are underway and will be reported elsewhere.

C. Tests of imaging quality

The DIMS diagnostic has been assembled as described above, and initial imaging tests showed excellent transmission and imaging properties of the DIMS system in the UV range. In Fig. 4(a) the properties of the achromatic triplet lenses were tested. The input fiber optic bundle was illuminated and the fibers were imaged on the CCD detector using the aligned triplets. A broadband light-emitting diode source was used for illumination with two $\Delta\lambda$=1.0 nm bandpass interference filters with central wavelengths at λ670.8 nm and λ433.9 nm. Figure 4(b) shows the results from initial spectral imaging tests that included the input optics, monochromator, and CCD detector. In this test, a 3600 gr/mm grating was used in the McPherson monochromator with d=25 μm slit, and a fluorescent lamp was used as a source of Hg lines λ=435.8, 404.7, 365.0, 313.2, 302.2 nm (in the rightmost panel a pen-ray Hg lamp was used in front of the monochromator slit to obtain λ=265.3 nm).

In conclusion, two new divertor imaging diagnostics are being developed for the liquid lithium divertor characterization on NSTX: a Ly_α diode array and an UV-VIS-NIR high-resolution spectrometer. These diagnostics will provide recycling and impurity particle flux measurements for the LLD protection and performance evaluation.

ACKNOWLEDGMENTS

The authors would like to thank J. Abramson, P. Sichta, G. Tchilinguirian, G. Zimmer, D. LaBrie, T. Holoman, and G. Smalley (PPPL) for computer and technical support. Dr. M. G. Bell, Dr. B. Stratton (PPPL), and Dr. K. Tritz (Johns Hopkins U.) are acknowledged for technical discussions. The entire NSTX Team is acknowledged for research, plasma, and neutral beam operations. This work was performed under the auspices of the U.S. Department of Energy under Contract Nos. DE-AC52-07NA27344 and DE-AC02-09CH11466.

[1] H. Kugel, M. Bell, J.-W. Ahn, J. Allain, R. Bell, J. Boedo, C. Bush, D. Gates, T. Gray, S. Kaye, R. Kaita, B. LeBlanc, R. Maingi, R. Majeski, D. Mansfield, J. Menard, D. Mueller, M. Ono, S. Paul, R. Raman, A. Roquemore, P. Ross, S. Sabbagh, H. Schneider, C. Skinner, V. Soukhanovskii, T. Stevenson, J. Timberlake, W. Wampler, and L. Zakharov, Phys. Plasmas **15**, 056118 (2008).
[2] M. Bell, H. Kugel, R. Kaita, L. Zakharov, H. Schneider, B. LeBlanc, D. Mansfield, R. Bell, R. Maingi, S. Ding, S. Kaye, S. Paul, S. Gerhardt, J. Canik, J. Hosea, and G. Taylor, Plasma Phys. Controlled Fusion **51**, 124054 (2009).
[3] H. Kugel, M. Bell, L. Berzak, A. Brooks, R. Ellis, S. Gerhardt, H. Harjes, R. Kaita, J. Kallman, R. Maingi, R. Majeski, D. Mansfield, J. Menard, R. Nygren, V. Soukhanovskii, D. Stotler, P. Wakeland, and L. Zakharov, Fusion Eng. Des. **84**, 1125 (2009).
[4] J. Kallman, M. A. Jaworski, R. Kaita, H. Kugel, and T. K. Gray, Rev. Sci. Instrum. **81**, 10E117 (2010).
[5] R. E. Bell and R. Feder, Rev. Sci. Instrum. **81**, 10D724 (2010).
[6] E. M. Hollmann, A. Y. Pigarov, and R. P. Doerner, Rev. Sci. Instrum. **74**, 3984 (2003).
[7] K.-D. Zastrow, S. R. Keatings, L. Marot, M. G. O'Mullane, G. de Temmerman, and JET-EFDA Contributors, Rev. Sci. Instrum. **79**, 10F527 (2008).
[8] R. Kaita, R. Majeski, R. Doerner, T. Gray, H. Kugel, T. Lynch, R. Maingi, D. Mansfield, V. Soukhanovskii, J. Spaleta, J. Timberlake, and L. Zakharov, J. Nucl. Mater. **363–365**, 1231 (2007).
[9] M. Rasigni and G. Rasigni, J. Opt. Soc. Am. **67**, 54 (1977).
[10] K. Behringer, J. Nucl. Mater. **145–147**, 145 (1987).
[11] R. D. Smirnov, A. Y. Pigarov, S. I. Krasheninnikov, T. D. Rognlien, V. A. Soukhanovskii, M. E. Rensink, R. Maingi, C. H. Skinner, D. P. Stotler, R. E. Bell, and H. W. Kugel, Contrib. Plasma Phys. **50**, 299 (2010).
[12] H. P. Summers, The ADAS User Manual, version 2.6. See http://adas.phys.strath.ac.uk (2004).
[13] V. Soukhanovskii, A. Roquemore, C. Skinner, J. Menard, H. Kugel, D. Johnson, R. Maingi, S. Sabbagh, and F. Paoletti, Rev. Sci. Instrum. **74**, 2094 (2003).
[14] I. Furno, H. Weisen, J. Mlynar, R. Pitts, X. Llobet, Ph. Marmillod, and G. Pochon, Rev. Sci. Instrum. **70**, 4552 (1999).
[15] R. Boivin, J. Goetz, E. Marmar, J. Rice, and J. Terry, Rev. Sci. Instrum. **70**, 260 (1999).
[16] D. Stutman, M. Finkenthal, V. Soukhanovskii, M. May, H. Moos, and R. Kaita, Rev. Sci. Instrum. **70**, 572 (1999).
[17] V. Soukhanovskii, D. Stutman, M. Iovea, M. Finkenthal, H. Moos, T. Munsat, B. Jones, D. Hoffman, R. Kaita, and R. Majeski, Rev. Sci. Instrum. **72**, 737 (2001).
[18] D. Gray, S. Luckhardt, L. Chousal, G. Gunner, A. Kellman, and D. Whyte, Rev. Sci. Instrum. **75**, 376 (2004).
[19] A. Degeling, H. Weisen, A. Zabolotsky, B. Duval, R. Pitts, M. Wischmeier, P. Lavanchy, P. Marmillod, and G. Pochon, Rev. Sci. Instrum. **75**, 4139 (2004).
[20] C. Suzuki, B. Peterson, and K. Ida, Rev. Sci. Instrum. **75**, 4142 (2004).
[21] M. Reinke and I. Hutchinson, Rev. Sci. Instrum. **79**, 10F306 (2008).
[22] V. Soukhanovskii, D. Johnson, R. Kaita, and A. Roquemore, Rev. Sci. Instrum. **77**, 10F539 (2006).
[23] V. Soukhanovskii, Rev. Sci. Instrum. **79**, 10F539 (2008).
[24] V. Soukhanovskii, R. Maingi, D. Gates, J. Menard, S. Paul, R. Raman, A. Roquemore, M. Bell, R. Bell, J. Boedo, C. Bush, R. Kaita, H. Kugel, B. LeBlanc, and D. Mueller, Phys. Plasmas **16**, 022501 (2009).
[25] V. Soukhanovskii, R. Maingi, D. Gates, J. Menard, S. Paul, R. Raman, A. Roquemore, R. Bell, C. Bush, R. Kaita, H. Kugel, B. LeBlanc, and D. Mueller, Nucl. Fusion **49**, 095025 (2009).